Journal of Molecular Liquids 394 (2024) 123587

Contents lists available at ScienceDirect

Journal of Molecular Liquids

journal homepage: www.elsevier.com/locate/molliq

Modulation of the NLO properties of *p*-coumaric acid by the solvent effects and proton dissociation

Marcus V.A. Damasceno [a], Antônio R. Cunha [b], Patricio F. Provasi [c], Gabriel I. Pagola [d], Marcelo Siqueira [e], Vinícius Manzoni [f], Rodrigo Gester [g,h,*], Sylvio Canuto [h]

[a] Faculdade de Ciências Biológicas, Agrárias, Engenharia e da Saúde, Universidade do Estado de Mato Grosso, Tangará da Serra-MT, 78300-000, Brazil
[b] Universidade Federal do Maranhão, Balsas-MA, 05314970, Brazil
[c] Department of Physics and CONICET - University of Northeaster, Instituto de Modelado e Innovación Tecnológica (IMIT), AV. Libertad 5500, W 3404 AAS Corrientes, Argentina
[d] Universidad de Buenos Aires, Facultad de Ciencias Exactas y Naturales, Departamento de Física, and CONICET - Universidad de Buenos Aires, Instituto de Física de Buenos Aires (IFIBA), Ciudad Universitaria, 1428, Buenos Aires, Argentina
[e] Curso de Física, Universidade Federal do Amapá, Macapá, AP, Brazil
[f] Instituto de Física, Universidade Federal de Alagoas, 57072-970 Maceió-AL, Brazil
[g] Instituto de Ciências Exatas, Universidade Federal do Sul e Sudeste do Pará, Marabá-PA, 68507-590, Brazil
[h] Instituto de Física, Universidade de São Paulo, Rua do Matão 1371, 05588-090, São Paulo, SP, Brazil

ARTICLE INFO

Keywords:
UV-Vis spectra
Thermochemistry
NLO properties
Solvent effects
Coupled Custer methods
Monte Carlo simulations

ABSTRACT

Solute-solvent interactions and deprotonation effects have been related to second-order nonlinear optical response modulators. This work takes advantage of sequential Monte Carlo/Quantum mechanics together with Time-Dependent Density Functional Theory, Coupled Cluster methods, and the hyper-Rayleigh scattering formalism to investigate how these effects influence the stability and optical response of *p*-coumaric acid (pCA) and its anionic and diionic forms. The solvent influences the chromophores in different ways, inducing bathochromic and hypsochromic solvatochromism so for the neutral pCA molecule as for its deprotonated derivatives. The results indicate a high sensitivity of the nonlinear optics (NLO) parameters with relation to proton dissociation. Ionization of the carboxyl group produces the lowest values of the first frequency-dependent hyperpolarizability (β_{HRS}), while phenolic deprotonation leads to the highest values. The results show that proton removal can be used as a switch that modulates the NLO response within a wide range of values ($159.15 \leq \beta_{HRS} \leq 4393.97$ au) greater than those reported for reference NLO chromophores like urea (37.3 au) and *p*-nitroaniline (74.3 au). Thermochemical analysis of enthalpies and Gibbs free energies indicate that both monoionic forms of the pCA molecule are the most stable in gas or water solvents. Furthermore, these structures represent the limits of NLO modulation in the gas and solvent phases. Analysis of the projected density of states and mapping of the molecular electrostatic potential indicate that increased contributions from conduction electrons found in the aromatic ring are the mechanism by which deprotonation enhances the NLO response. All the results show that ionic pCA forms are promising in the functionalization of optoelectronic devices.

1. Introduction

There are two main strategies to amplify a given molecular property. First, chemical synthesis, in which known molecular groups are inserted into the molecular body to enhance this effect [1]. Second, to use the solvent as a means of producing polarization and specific intermolecular interactions like Coulomb and van der Waals forces to control this property [2–4]. This last method can affect the conformational equilibrium relative to the gas phase [5,6], which can be explained, in general, by the difference in free energy between conformations in solution, mainly in polar solvents, where structures with a stronger dipole moment are expected to be favored [7].

However, among the effects mentioned above, molecular solvatochromism is the best-known solvent contribution. This effect is the result of the action of the solvent on the shape, intensity, and position of the transition lines of the absorption and emission spectra [2,3,8–10].

* Corresponding author.
E-mail address: gester@unifesspa.edu.br (R. Gester).

https://doi.org/10.1016/j.molliq.2023.123587
Received 14 June 2023; Received in revised form 10 November 2023; Accepted 13 November 2023
Available online 20 November 2023

They are said to be bathochromic or hypsochromic if the solvent shifts a given excitation towards lower or higher energies, respectively, and just to get a general idea, knowledge of this behavior is essential if one wishes to propose optical applications such as bioprobes and sensors [11,12].

On the other hand, although a mature knowledge of the treatment of properties related to electronic excitations is currently shared, the molecular NLO response remains a challenge. Knowledge of these effects is relatively recent, only observed after the discovery of the first high-power laser in 1960 by Mainman [13]. Since then, various electro-optical devices such as organic light-emitting diodes, solar cells, and sensors have been proposed. The advantage of such devices is that they propagate some information as fast as the speed of light allows, giving greater efficiency compared to conventional electronic devices [14,15].

Nowadays, in the fabrication of NLO devices, organic chromophores are known to be more efficient than inorganic dyes as they better resist the breakdown threshold imposed by high-power light. In addition, organic dyes are easily manipulated by standard chemical synthesis procedures, allowing an alternative to adjust the NLO response [16,17]. Therefore, the materials science community has put a lot of effort into planning how to harness, improve, and control NLO behavior in organic chromophores [18]. After a decade of NLO, most of these theoretical advances that were compiled in a review by Ratner and collaborators [19], are being systematically updated [20,21].

In this direction, two decades ago, Wang [22] and Nisic [23] demonstrated how the modulation of second-order NLO properties can be efficiently improved by taking advantage of simple protonation/deprotonation procedures. In particular, this work has opened up a wide range of possibilities. For example, it has recently been shown that simple deprotonation effects and solute-solvent interactions can change the second-order NLO behavior of azo dyes to giant values of the first hyperpolarizability [24,25]. However, practically no discussion on the effects of proton dissociation on organic dyes deals with their stability, which could be a worrying sign, considering that the stability of these dyes depends on various factors, for example, the pH of the medium, and its polarity, among others.

Within the scenario described above, pCA emerges as an interesting and promising case study (see Fig. 1). This organic dye is well known for its recognized biological use as an antioxidant, anti-inflammatory, and antiplatelet agent, as well as against human diseases such as diabetes and cancer [26]. Regarding its physicochemical properties, it has been experimentally demonstrated how the simple dissociation of mono and diprotons can cause a strong change in the ultraviolet-visible (UV-Vis) spectrum. However, the second-order NLO response depends linearly on the optical gap ($\beta \propto \lambda_{max}$) [19], which means that the way pCA molecules interact with the light can be significantly altered.

Thus, based on molecular modeling techniques and quantum mechanical approximation, this work presents for the first time a systematic thermochemical discussion on the formation and stability of monoionic and diionic forms of pCA molecules under gaseous and liquid conditions using different levels of solvation models. Special attention is paid to linear and non-linear optical properties.

2. Methodology

The structure in the gas phase (see Fig. 1) and the electronic properties of pCA and the monoanionic (9-pCA$^-$ and 1-pCA$^-$) and dianionic (pCA^{-2}) were determined by performing density functional theory (DFT) calculations [27–29] using the B3LYP [30,31] exchange-correlation functional, and Møller-Plesset second-order perturbation theory (MP2) [32]. These methods were used in combination with the Pople basis set, 6-311+G(*d,p*) [33,34]. The electronic excitation energies were determined by applying the time-dependent density functional theory (TD-DFT) [37] with the CAM-B3LYP functional implemented in the Gaussian 09 [38] program.

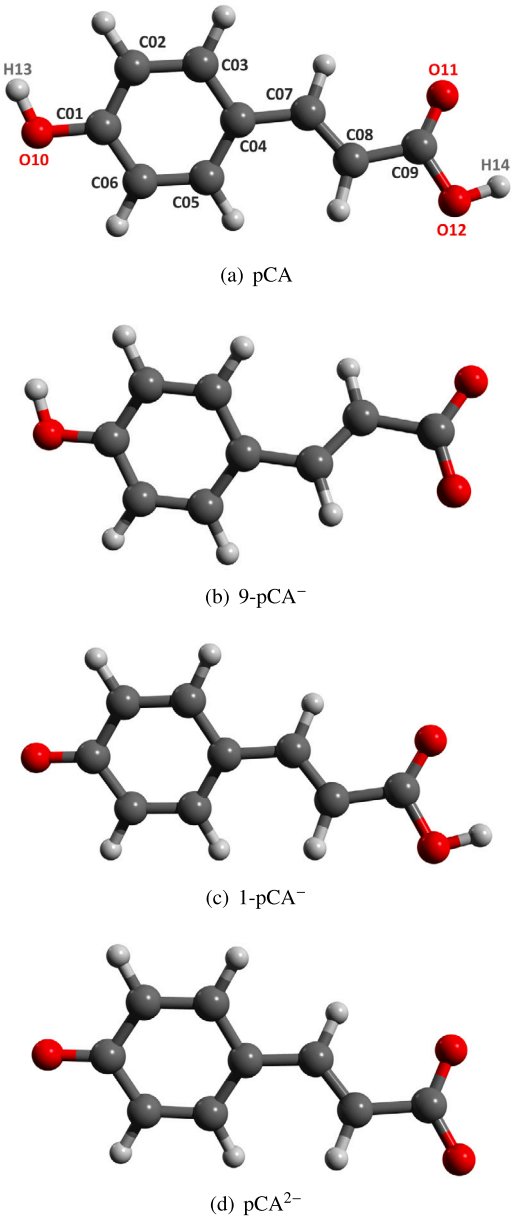

(a) pCA

(b) 9-pCA$^-$

(c) 1-pCA$^-$

(d) pCA^{2-}

Fig. 1. Geometries of the *p*-coumaric acid forms obtained at the B3LYP/6-311G++(*d,p*) at gas-phase conditions.

The analysis of the electronic properties of the pCA in aqueous solution was based on the continuous and discrete models of the solvent. We use the continuum polarized model (PCM) [39,40] and for the discrete model we performed the sequential procedure of quantum mechanics and molecular mechanics, S-QM/MM [41–43].

In the S-QM/MM procedure, initially, the liquid phase configurations are sampled from molecular simulations, and after statistical analysis, only configurations with less than 10% statistical correlation are selected and subjected to quantum mechanics calculations. In our study, we used the Monte Carlo (MC) method with the Metropolis sampling technique [44] to perform the liquid simulation. This sampling was performed separately for structures pCA, 1-pCA$^-$, 9-pCA$^-$, and pCA^{2-} in water. We assume that the pCA structures in water are not significantly modified concerning those in the gas phase. Thus, the structures (optimized at the B3LYP/6-311+G(*d,p*) level) remained rigid during MC sampling generated by the DICE [45]. The MC sampling was carried out under standard conditions ($p = 1$ atm; $T = 298$ K) in the *NpT* ensemble for a system with one pCA molecule and $N = 1000$ molecules

of water in a cube box of length $L \approx 31.14$ Å and applying periodic boundary conditions and image method. In the pairwise energy calculation, the pCA interacts with all water molecules within a separation from the center of mass that is smaller than the cutoff radius $r_c = L/2$ (i.e., approximately 15.57 Å in the studied case). For separations greater than r_c, the long-range correction of the potential energy [46] was calculated. In each simulation, 15×10^6 MC steps were performed in the thermalization stage and 37×10^6 MC steps in the production stage.

The solute-water and water-water interactions were described by a Lennard-Jones intermolecular potential plus a Coulombic term described by the interactions between atomic point charges. Water was represented by the SPC model [47]. The choice of Lennard-Jones parameters for the pCA molecule was driven by the OPLS force field [48]. The Gibbs free energy of hydration, ΔG_{solv}, was calculated using the PCM.

The NLO response of matter, when high power of field E light interacts with a chromophore of field E, the total dipole moment becomes

$$\mu_{\text{ind}} = \mu_p + \sum_{j}^{x,y,z} \alpha_{ij} E_j + \frac{1}{2!} \sum_{j,k}^{x,y,z} \beta_{ijk} E_j E_k + \ldots \quad (1)$$

In this expression, while μ_p is the permanent dipole moment, α is a tensor of rank 2 relevant in structural chemistry. However, since this tensor is not the focus of the present work, it will not be evaluated. In contrast, The main focus is on the frequency-dependent first hyperpolarizability (β_{HRS}) obtained within the hyper-Rayleigh scattering formalism [50,52], in which the tensor's components can be handled to obtain the dipolar ($\Phi_{J=1}$) and octupolar ($\Phi_{J=3}$) contributions to the NLO response, besides the depolarization ratio (DR). Many authors generally combine information extracted from these parameters constructing scales that classify chromophores according to their dipolar-octupolar architecture [50].

Regarding the calculation of NLO properties, Coupled Cluster (CC) methods are considered to be state-of-the-art among electronic structure methods and are often used as a reference to analyze the performance of other electronic structure methods [51]. Therefore, we used CCSD and CC2 and some DFT-based methods with standard base set 6-311++G(d,p) [33,34] to analyze the NLO response of pCA molecules. The choice of this particular basis set is based on previous work showing that small basis sets can describe NLO parameters if polarizable and diffuse functions are taken into account. Particularly, de Wergifosse and Champagne investigated the dependence of the basis set together CC methods using some push-pull π-conjugated systems as a test case [35]. According to their results, a better balance between precision and computational efforts was achieved using the 6-31+G(d) to describe systems that present alternated single and triple C-C bonds. On the other hand, 6-31G(d) is enough to describe polymer links (=C-C=C-C=). Similar results have been found studying p-quinodimethane dyes [36]. Moreover, we also performed our own investigation on the basis set at CCSD level of calculations in the gas phase (see **Table SS**). As respected, the smallest 6-31G basis set is enough to approach the results obtained using the greatest 6-311++G** functions.

For the contributions of the solvent to the quantum mechanical properties, we take advantage of four solvation models:

- **PCM:** The Integral-Equation Formalism of the polarizable continuum model, [39,40] that encloses the solute in a cavity that conforms to the shape of the molecule and represents the solvent as a continuum environment with a dielectric constant ϵ.
- **ASEC:** The solvent surrounding the pCA form is represented by the superposition of 100 uncorrelated solvent structures extracted from Monte Carlo Simulations, in which the atoms of solvent molecules were replaced by their normalized atomic charges generating an Average Solvent Electrostatic Configuration (ASEC) [49]. Each selected solvent structure accounts for the 300 water molecules nearest to the solute within a radius of 13Å, totalizing 90000 enfolding point charges.
- **HB+PC** and **MS+PC:** While the former incorporates only the solute-solvent hydrogen bonds in the electrostatic field of the remaining 300 solvent molecules accounted for as point charges, the latter includes all of the micro-solvation shells. These proposals account for the closest specific solute-solvent interactions, from Van der Waals forces to electrostatic interactions of bulk molecules.

From the thermochemical point of view, the Gibbs Free Energies are recovered as:

$$\Delta G_g^{(1)} = G_g(x\text{-pCA}^-) + G_g(H^+) - G_g(\text{pCA})$$
$$\Delta G_g^{(2)} = G_g(\text{pCA}^{2-}) + G_g(H^+) - G_g(x\text{-pCA}^-) \quad (2)$$

where x = 9 or 1. Moreover, the involved pK_a are obtained using the relations:

$$pk_a^1 = \frac{\Delta G_{aq}^{(1)}}{RTln(10)} \quad \text{and} \quad pk_a^2 = \frac{\Delta G_{aq}^{(2)}}{RTln(10)} \quad (3)$$

where

$$\Delta G_{aq}^{(1)} = \Delta G_g^{(1)} + \Delta G_{solv}(x\text{-pCA}^-) + \Delta G_{solv}(H^+) - \Delta G(\text{pCA}) \quad (4)$$

and

$$\Delta G_{aq}^{(2)} = \Delta G_g^{(2)} + \Delta G_{solv}(\text{pCA}^{2-}) + \Delta G_{solv}(H^+) - \Delta G(x\text{-pCA}^-) \quad (5)$$

again with x =9 or 1.

Finally, although all quantum mechanics calculations were performed using Dalton [53] and Gaussian 09 [38] programs, the output analysis was carried out taking advantage of the Multiwfn code [54].

3. Results and discussion

3.1. Geometry optimization and relative stability of the isomers

Full geometry optimization and vibrational frequency calculations in gas phase of the neutral form of pCA, its unique deprotonated phenolate (1-pCA$^-$) (phenolate) and carboxylate (9-pCA$^-$), as well as its doubly deprotonated structure (pCA^{2-}) were performed at the B3LYP/6-311+G(*d,p*) level of the QM calculation (Table 1). All these calculations were also performed in water, using the solvent described by the PCM model with the same level of QM calculation. We find that all the optimized structures of the pCA compounds are flat and stable, in close agreement with the previous geometries obtained at the MP2 [55] and DFT [56,57] levels of calculation and crystallographic experimental data [58–60].

Initially, by comparing the geometries in the gas phase and aqueous solution, we observed that the effects of the solvent on the structural properties of pCA are small, with bond distances and angle variations less than 2%. Therefore, all the calculations for the pCA compounds were made considering the void structures. Theoretical data for the electronic energy, the Gibbs free energy, and the dipole moment of the pCA compounds in gas and in water are presented in **Table S1**.

Garcia-Prieto et al. [56] showed that four different forms of cis-trans isomerization can be proposed for the neutral form of pCA: (i) s-cis-anti; (ii) s-cis-syn; (iii) s-trans-anti, and (iv) s-trans-syn. They showed that, regardless of the medium used, the s-cis isomers are more stable compared to the s-trans isomers and identified the s-cis-anti isomer as the most stable in the gas phase and the s-cis-syn as its counterpart in solution. Therefore, we adopt the s-cis-syn isomer as the starting point of the geometry optimization calculations. The calculated value obtained for the gas phase dipole moment of pCA is 3.72 D, in close agreement with previous theoretical values [56,57].

Comparing the free energy in the gas phase, G_g, of the two isomeric forms with deprotonation, 9-pCA$^-$ and 1-pCA$^-$, we observe that the 1-pCA$^-$ isomer is 14.70 kcal/mol more stable compared to 9-pCA$^-$. However, in an aqueous solution, inversion is observed and the 9-pCA$^-$

Table 1
The free energy (in kcal/mol) for *p*-coumaric forms (pCA, 9-pCA$^-$, 1-pCA$^-$, and pCA^{2-}) involved in the first and second deprotonation processes in the gas phase. The geometries were optimized with B3LYP/6–311++G(*d,p*), and the corrections of zero-point, thermal, and enthalpy were obtained after the vibrational frequencies calculations.

Free energy in Gas phase, G_g	Values in kcal/mol
G_g(pCA)	-359880.17
G_g(9-pCA$^-$)	-359539.18
G_g(1-pCA$^-$)	-359553.88
G_g(H$^+$)	-5.4 [62]
ΔG_g(pCA → 9-pCA$^-$ + G_gH$^+$)	335.59
ΔG_g(pCA → 1-pCA$^-$ + H$^+$)	320.89
ΔG_g(9-pCA$^-$ → pCA^{2-} + H$^+$)	387.53
ΔG_g(1-pCA$^-$ → pCA^{2-} + H$^+$)	402.23

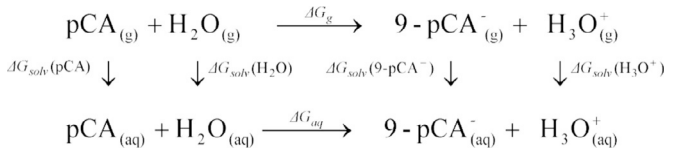

(a) **Scheme 1**

Fig. 2. The thermodynamic cycle with the acid-base reaction between the pCA molecules and water in the gas phase and in aqueous solution.

isomer is slightly more stable than the 1-pCA$^-$ isomer (Δ(1-pCA$^-$ → 9-pCA$^-$ = 1.51 kcal/mol). This small difference in the free energy of the isomers in water leads to a coupled system of two-monoanios with both phenolate and carboxylate isomers at room temperature ($RT \approx 0.6$ kcal/mol). To better define this system, a study of pCA acidity constants in water is carried out as will be seen below. We also analyze the structure of the form double anion of pCA (pCA^{2-} see Fig. 1 and **Table S1**. It is important to stress that pCA^{2-} is unstable concerning autoionization and cannot exist in the gas phase [61]. In water, this divalent anion form is stable with respect to self-ionization and may exist. The calculated dipole moment of pCA^{2-} in gas is 5.15 D.

As mentioned above, the solvent effects on the geometric parameters of the pCA shapes are minimal, however, deprotonation leads to a considerable variation in these parameters. In all deprotonated forms, a decrease of ~ 8% (in the gas phase) and ~ 7% (in aqueous solution) can be noted in the C-O bond lengths of the deprotonation sites relative to the neutral form. Comparing the two isomeric forms with deprotonation, we observe that the 1-pCA$^-$ have a slight quinoidal character of the phenolic ring, with the C2-C3 and C5-C6 bonds being lower (around 2%) in comparison with the corresponding to 9-pCA$^-$. This result is in agreement with previous studies carried out by García-Prieto et al. [56].

Another interesting point is the charge redistribution and electronic polarization of the pCA ionic forms caused by the solvent effect. This aspect can be evidenced by the large difference between the dipole moment in the gas phase (μ_g) and in the aqueous solution (μ_{aq}) as shown in **Table S1**. We observed 36%, 32%, 75%, and 31% increases in dipole moments of pCA, 9-pCA$^-$, 1-pCA$^-$ and pCA^{2-} in water compared to the gas phase. It is interesting to note that the increase in the dipole moment of the phenolate anion is more than twice that of the carboxylate anion. This large difference in the dipole moment of the isomers can be seen as a consequence of the charge distribution of the solute in water. While in the carboxylate, the two oxygen atoms at the carboxylate end O11 and O12 have almost the same charge (about -0.84 in the gas phase and -0.92 in water, an increase of ~ 9%), which are more negative than phenolic oxygen, O10 (-0.67 in the gas phase and -0.69 in water, an increase of ~ 3%). In the case of the phenolate form, the three oxygen atoms O10, O11, and O12 have similar charges in the gas phase (about -0.76 for O10, -0.72 for O11, and -0.69 for O12), but they differed in water with the negative charge most located in deprotonated oxygen (around -0.72 for O11 and O12 and -0.85 for O10). Thus, the effect of the solvent on the electronic polarization of two isomers leads to a delocalization of the negative charge at different ends of the isomers. In the case of the carboxylate, this charge is located in the COO$^-$ group, while in the phenolate it is located in the PhO$^-$ group. This result strongly indicates that the effect of the solvent on the electronic polarization of this type of compound is an essential factor in the determination of atomic charges and must be taken into account for an adequate description of their interaction with the solvent. This was observed by García-Prieto et al. [56], who studied the neutral and charged pCA forms in an aqueous solution using molecular dynamics simulations combined with the ASEP/MD procedure. They demonstrated that the interaction of both 1-pCA$^-$ and 9-pCA$^-$ with solvent molecules alters the relative stability of the isomers, where in aqueous solution, the carboxylate is more stable than the phenolate form.

3.2. Theoretical deprotonation process of p-coumaric in gas phase and in water

To further analyze the *p*-coumaric acid/base balance in water, we initially calculated the gas phase free energy of the first and second deprotonation using the free energy of the species involved as presented in the Eq. (2). The free energy of the neutral form of pCA and its deprotonated forms (1-pCA$^-$, 9-pCA$^-$ and pCA^{2-}) in the gas phase was calculated by adding the electronic energy with zero point, thermal, and enthalpy corrections. For H$^+$, we used the value of G_g(H$^+$) = −5.4 kcal/mol, reported previously [62]. Thus, the values calculated for the first deprotonation process, ΔG_g(pCA → 9-pCA$^-$ + H$^+$) and ΔG_g(pCA → 1-pC$^-$ + H$^+$), using Eq. (2) are 333.75 and 320.34 kcal/mol. Similarly, for the second deprotonation process, ΔG_g(9-pCA$^-$ → pCA^{2-} + H$^+$) and ΔG_g(1-pCA$^-$ → pCA^{2-} + H$^+$), we obtained the values of 387.53 and 402.23 kcal/mol using Eq. (2) (more details in **Table S2**). For the pK_a calculations, we use these values in the Eq. (5) as will be seen below.

By using the thermodynamic cycles shown in Fig. 2, the values for ΔG_g (gas phase free energy of the first and second deprotonation), $\Delta G_{solv}(X)$ (standard solvation free energies for the proton X = H$^+$, pCA, 9-pCA$^-$, 1-pCA$^-$ and pCA^{2-}), we determined the values for the first (pK_{a1}) and second (pK_{a2}) acidity constants of pCA in water. For the proton, X = H$^+$, several studies have been carried out to determine its standard free energies of solvation in water [63–69]. Here, we decided to use the experimental value of ΔG_{solv}(H$^+$) = 265.9 kcal/mol obtained by Tissandier it et al. [68], under standard conditions (1.0 M concentration in the gas phase). For the other species, X = pCA, 9-pCA$^-$, 1-pCA$^-$, and pCA^{2-}, $\Delta G_{solv}(X)$ were performed with QM calculations, where the effect of solvent was included using the PCM [39]. The three contributions of the standard free energies of solvation, $\Delta G_{ele}(X)$, $\Delta G_{vdW}(X)$, and $\Delta G_{cav}(X)$, as well as the total values of the standard free energy of solvation of each species, that is $\Delta G_{solv}(X) = \Delta G_{ele}(X) + \Delta G_{vdW}(X) + \Delta G_{cav}(X)$, that are shown in Table 2.

The results obtained for standard solvation free energies, $\Delta G_{solv}(X)$, for X = pCA, 9-pCA$^-$, 1-pCA$^-$, and pCA^{2-}, in water are -15.18, -78.18, -59.17 and -185.81 kcal/mol, respectively. Note that the relative free energy of solvation ($\Delta\Delta G_{solv} = \Delta G_{solv}$(1-pCA$^-$) − ΔG_{solv}(9 -pCA $^-$)) of the 9-pCA$^-$ and 1-pCA$^-$ isomers is 19 kcal/mol, indicating that the 9-pCA$^-$ isomer is more stable in water compared to 1-pCA$^-$. This result is in agreement with our QM results discussed in this section and with those by García-Prieto et al. [56]. The calculated values of the standard deprotonation free energies of pCA in aqueous solution for the first deprotonation are ΔG_{aq}(pCA → 9-pCA$^-$ + H$^+$) = 6.69 and ΔG_{aq}(pCA → 1-pCA$^-$ + H$^+$) = 11.00 kcal/mol, obtained using Fig. 2. These values for the second deprotonation are ΔG_{aq}(9-pCA$^-$ → pCA^{2-} + H$^+$) = 14.00 and ΔG_{aq}(1-pCA$^-$ → pCA^{2-} + H$^+$) = 9.69 kcal/mol, obtained using Fig. 2. Therefore, the existence of two isomeric forms with deprotonation for pCA leads to two pathways of two-proton stepwise disso-

Table 2
Solvation-free energies in (kcal/mol) of *p*-coumaric forms (pCA, 9-pCA$^-$, and 1-pCA$^-$) involved in the first deprotonation process in water according to the equilibrium reaction shown in Scheme 1. The values were calculated using QM calculation with HF/6-31+G(*d*)/PCM/UAHF.

Free energy	X = pCA	X = 9-pCA$^-$	X = 1-pCA$^-$	X = pCA^{2-}
$\Delta G_{ele}(X)$	-18.19	-80.68	-62.00	-188.14
$\Delta G_{vdW}(X)$	-18.92	-18.71	-18.51	-18.28
$\Delta G_{cav}(X)$	21.94	21.21	21.33	20.61
$\Delta G_{solv}(X)$	-15.18	-78.18	-59.17	-185.81
Scheme 1	ΔG_g	ΔG_{aq}	pK_a	pK_a [Exp.]
(pCA → 9-pCA$^-$ + H$^+$)	335.59	6.69	4.90	4.36 [70], 4.6 [71]
(pCA → 1-pCA$^-$ + H$^+$)	320.89	11.00	8.06	4.36 [70], 4.6 [71]
Scheme 2				
(9-pCA$^-$ → pCA^{2-} + H$^+$)	387.53	14.00	10.26	8.98 [70], 9.3 [71]
(1-pCA$^-$ → pCA^{2-} + H$^+$)	402.23	9.69	7.10	8.98 [70], 9.3 [71]

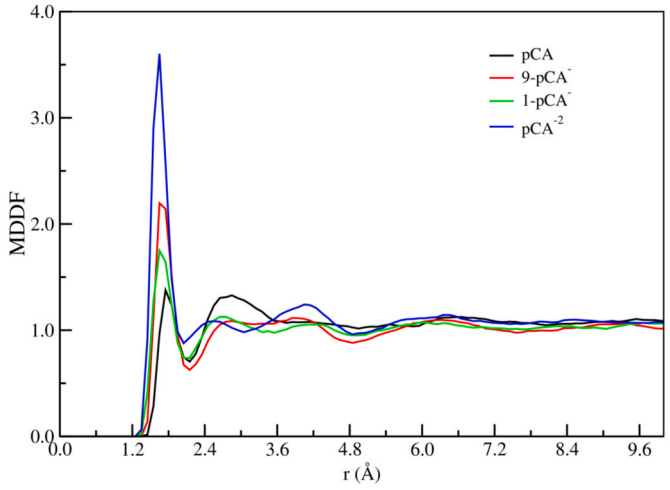

Fig. 3. Minimum distance distribution function (MDDF) between p-coumaric forms (pCA, 9-pCA$^-$, 1-pCA$^-$, and pCA^{2-}) and the water molecules obtained from MC simulations.

ciation, with a free energy difference between the two pathways of about 4.3 kcal/mol. This difference in deprotonation free energy leads to two values for the pK_a of pCA in aqueous solution (pK_{a1}(pCA → 9-pCA$^-$ + H$^+$) = 4.90 and pK_{a1}(pCA → 1-pCA$^-$ + H$^+$) = 8.06 kcal/mol) for the first deprotonation and pK_{a2}(9-pCA$^-$ → pCA^{2-} + H$^+$) = 10.26 and pK_{a2}(1-pCA– → pCA^{2-} + H$^+$) = 7.10 kcal/mol) for the second deprotonation. The best comparison between the calculated values for pK_{a1}(4.90 and 8.06 kcal/mol) and pK_{a2}(10.26 and 7.10 kcal/mol) and experimental data (pK_{a1} = 4.36 kcal/mol [70] with direct dissociation pCA → 9-pCA$^-$ + H$^+$ for the first deprotonation and 9-pCA$^-$ → pCA $^{2-}$ + H$^+$ for the second deprotonation process. This result leads to the conclusion that the first deprotonation of pCA in water occurs at position 9, that is, in the COOH while the second deprotonation a occurs at position 1, *i.e.*, in the PhOH group, results in the two-proton stepwise dissociation pathway (pCA → 9-pCA $^-$ + H$^+$ → pCA $^{2-}$ + 2H$^+$)$_{aq}$.

3.3. Structure and hydrogen bonding in the p-coumaric-water solution

As discussed above, the effects of the solvent on the electronic polarization of pCA in neutral and deprotonated forms are essential for building solvation models to fully describe its interaction with the solvent. The liquid structure around the molecules charged by a polar solvent like water is probably more significant than the neutral molecules. Therefore, the solvation shells surrounding the pCA forms in all simulated systems were analyzed using the Minimum Distance Distribution Function (MDDF) [88] between solute and water molecules.

As shown in Fig. 3 and **Table S3**, similar MDDF profiles are observed for the pCA forms, indicating identical structures of solvation shells. However, a comparison among the MDDF profiles suggests that the arrangement of water molecules around each pCA system is different. The MDDF profiles show a more structured micro-solvation layer than the first and second solvation layers. This micro-solvation layer is observed starting at 1.2 Å and ending at 2.2 Å, containing approximately 6, 9, 8, and 11 water molecules around pCA, 9-pCA$^-$, 1-pCA$^-$, and pCA^{2-}, respectively. It has precisely the water molecules about to participate in the hydrogen bonds between the solute and the solvent.

The first hydration layer is observed in the range from 2.2 to 3.8 Å. Integration to 3.8 Å encloses 33, 27, 30, and 24 water molecules around pCA, 9-pCA$^-$, 1-pCA$^-$ and pCA^{2-}, respectively. The second save starts at 4.8 Å and extends to about 5.0 Å. By integrating the MDDF profiles over the region of the micro solvation layer, as well as the first and second solvation layers, it was determined that there are about 61, 62, 62, and 64 water molecules present around pCA, 9-pCA$^-$, 1-pCA$^-$ and pCA^{2-}, respectively. The structural properties obtained from the simulation analyses are summarized in **Table S1**. As expected, due to charge redistribution and electronic polarization of the charged forms, the solvation shell surrounding the species with a -2 charge had the largest number of water molecules, followed by those with a -1 charge and finally those that had a charge of 0. This tendency to increase the number of water molecules around the species is also observed in the microsolvation layer, since the simulation analyses returned more hydrogen-bonded water molecules with the species charge equal to -2 than with charge -1, as will be discussed later.

To better compare hydrogen bonding (HB) in neutral and charged species, we employ the order (a simple DICE tool) [89] to investigate these interactions between the pCA species and the molecules of water. The pCA has three acceptors (O1, O2, and O3) and two donors (H1 and H2) of the HB. HBs are obtained using a geometric distance (radial $R_{O\cdots O} \leq 3.25$ Å and angular O$\hat{O}$H ≤ 40°) and energy criteria ($E_{ij} \leq -0.01$ kcal/mol) [90,91]. We found an average of 3.8, 6.5, 4.4, and 5.6 HBs formed between the pCA forms (pCA, 9-pCA$^-$, 1-pCA$^-$ and pCA^{2-}) and water molecules, respectively. The calculated interaction energies for these hydrogen bonds are -5.3, -11.9, -7.9, and -15.6 kcal/mol, respectively. As we can see, there are obvious differences between the hydrogen bonding properties of the neutral and charged (single and doubly deprotonated) forms. The number and energy (in modulus) of H bonds in pCA structures are highest in pCA^{2-}, followed by 9-pCA$^-$ and 1-pCA$^-$, and finally by the PCA. In the case of the individually deprotonated isomers, these properties of 9-pCA$^-$ are much stronger compared to those of 1-pCA$^-$, indicating that 9-pCA$^-$ has strong HB interactions with water molecules.

3.4. Absorption spectra analysis

Table 3 and Fig. 4 show, respectively, the data for the ultraviolet-visible (UV-Vis) spectra of pCA molecules considering implicit and ex-

Table 3
Solvent effect on the $\pi - \pi^*$ excitation of *p*-coumaric forms. All values for wavelength (λ/nm) and oscillator strength (O.S.) are obtained at the TD-CAM-B3LYP/6-311++G(d,p) level of theory using different solvent models.

	Model	λ (nm)	O.S.	Exp.(nm)
pCA	Gas	282.6	0.7	
	PCM	294.8	0.8	308 [92]
	ASEC	288.1	0.7	
	HB + PC	290.8	0.8	
	MS + PC	293.9	0.8	
1-pCA$^-$	Gas	360.5	0.9	
	PCM	367.7	1.1	356 [92]
	ASEC	343.4	0.9	
	HB + PC	346.5	1.0	
	MS + PC	348.5	1.0	
9-pCA$^-$	Gas	261.3	0.4	
	PCM	273.9	0.6	285 [92]
	ASEC	271.5	0.6	
	HB + PC	282.2	0.7	
	MS + PC	272.0	0.5	
pCA^{2-}	Gas	298.7	0.5	
	PCM	321.8	0.7	333 [93]
	ASEC	304.1	0.7	
	HB + PC	315.7	0.8	
	MS + PC	308.6	0.9	

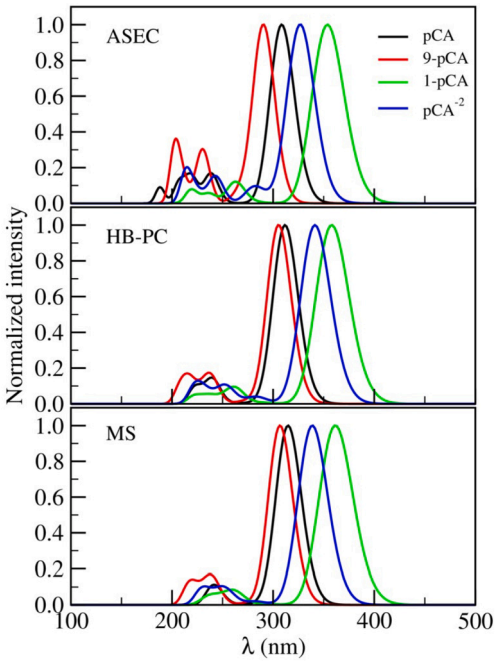

Fig. 4. The UV-Vis spectra calculated for pCA (black), 9-pCA$^-$ (red), 1-pCA$^-$ (green), and pCA^{2-} (blue) for different solvation models using the TD-CAM-B3LYP/6-311++G(*d,p*) level of quantum mechanics.

plicit solvation models and time-dependent DFT. The results allow us to analyze both the dissociation of protons and the effects of the solvent.

The UV-Vis spectra of the pCA molecules are assigned by a strong absorption band located in the visible region of the UV-Vis-Exp spectra. As for the gas phase results, although an experimental report is not allowed, the current results of TD-CAM-B3LYP indicate that proton dissociation shifts electronic excitations over a wide range of values. As an example, for the original pCA molecule, this absorption maximum is located at 301 nm, and analysis of the frontier molecular orbitals shown in Fig. 5 indicates that this spectral line is composed of a strong $\pi \rightarrow \pi^*$

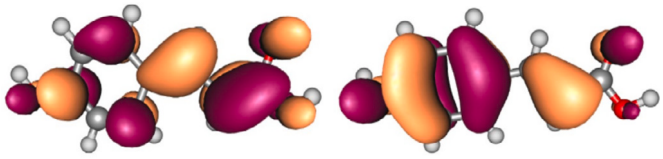

(a) LUMO (b) HOMO

Fig. 5. Illustration of the frontier molecular orbitals involved in the $\pi \rightarrow \pi^*$ transition: highest occupied molecular orbital (HOMO) and lowest unoccupied molecular orbital (LUMO) plotted using the CAM-B3LYP/6-311++G(*d,p*) level of theory.

symmetry. Regarding the loss of the proton, taking the pCA molecule as a reference, a bathochromic effect would be observed. From Table 3, in the gas phase, 1-pCA$^-$, 9-pCA$^-$, and pCA^{2-} molecules would present an optical space located respectively at 361, 261, and 299 nm.

On the other hand, the inclusion of the solvent introduces some particularities, affecting the order shown above, and indicating that it is dangerous to try to describe the liquid phase without proper modeling work. Based on experimental reports in an aqueous environment, the correct ordering for λ_{max} is 9-pCA$^-$ < pCA < pCA^{2-} < 1-pCA$^-$. In other words, the exchange between the pCA and 9-pCA$^-$ molecules must be taken into account. This effect has its origin in the different solvatochromes made for pCA and its deprotonated forms.

As an example, from gas to solvent, all solvation models indicate that the pCA molecule undergoes a bathochromic change. Electrostatic description, ASEC, and PCM show absorptions at 288 and 294 nm, which is clearly a redshift from gas phase excitation (283 nm). This trend is also corroborated by improving the level of modeling of the solvent. In this line, HB+PC and MS+PC include, respectively, the solute-solvent hydrogen bonds and the microsolvation layer in the electrostatic field of the 300 water molecules, being a more realistic description. These two models indicate absorptions at 291 ± 1 and 294 ± 1 nm, indicating $\sim 11 \pm 0.1$ nm as a bathochromic effect.

However, in contrast to the pCA solvatochromism, all its deprotonated forms show a hypsochromic effect in a solvent. For 9-pCA$^-$, which lost its proton from the carbonyl group, both HB+PC, and MS+PC give values at 282 and 272 nm which are in agreement with the experiment, 308 nm [92]. This displacement, although moderate, is enough to invert the relative positions between the transitions $\pi \rightarrow \pi^*$ between pCA and 9-pCA$^-$ chromophores with respect to the gas phase.

Similarly, the remaining two chromophores also undergo hypsochromic effects from the gaseous to the liquid medium. For the pCA^{2-} molecule, the ASEC solvation model predicts the maximum to be at 304 nm, in good agreement with the experimental data of 333 nm [92], and indicating a smooth redshift of 5 nm from the gas phase. The PCM, HB+PC, and MS+PC solvation models show the same behavior.

Finally, the blue shift is visible for the 1-pCA$^-$ form. The experimental report for the lowest $\pi \rightarrow \pi^*$ excitations is 356 nm [93], which is in excellent agreement with some theoretical predictions set out in Table 3. ASEC and HB+PC estimate 343 and 347 ± 1 nm, respectively. These values suggest blue changes around 18 and 14 nm. Although the other models overestimate λ_{max}, they confirm molecular hypochromics.

To appreciate it, it is possible to see the results with B3LYP in **Table S4 and Fig. S1** that shows a behavior similar to that obtained with CAM-B3LYP. However, the B3LYP method presents results slightly shifted towards high energies, indicating that the lack of long-range interactions tends to overestimate the absorption energies.

3.5. *Frequency-dependent first hyperpolarizability*

Table 4 presents the results of the NLO response of pCA molecules considering different degrees of quantum mechanics using the 6-311++G(*d,p*) basis set. First considering the pCA molecule under gas

Table 4
The frequency-dependent ($\omega = 1064$ nm) first hyperpolarizabilities (β_{HRS}/au) obtained within the hyper-Rayleigh scattering formalism for different solvation models, quantum mechanics approximations and the 6-311++G(*d,p*) basis set.

Complex	Model	CCSD	CC2	CAM-B3LYP	ωB97XD	B3LYP
9-pCA$^-$	Gas	159.55	284.80	164	152	369
	ASEC	159.15	235.45	1028	990	1377
	PCM			949	932	1281
pCA	Gas	1097.70	1443.54	1373	1301	1708
	ASEC	1098.46	1483.45	1702	1611	2095
	PCM			2290	2159	2994
pCA^{2-}	Gas	1673.18	2228.77	1902	1809	4567
	ASEC	1643.44	2208.27	2359	2231	2511
	PCM			3568	3358	2095
1-pCA$^-$	Gas	4191.18	4495.79	3446	3500	2782
	ASEC	4393.97	4906.18	3297	3252	2862
	PCM			6105	6039	5193

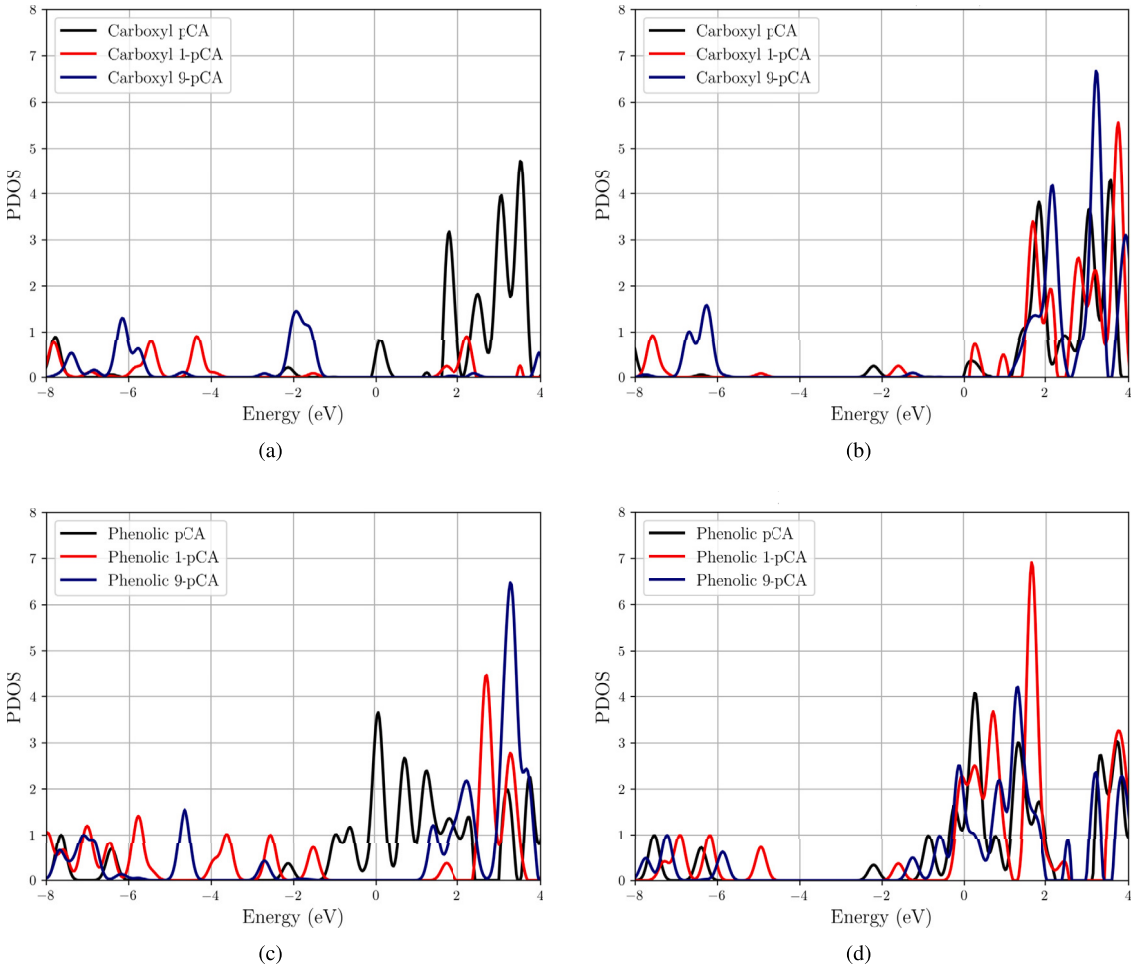

Fig. 6. PDOS os pCA molecules and their changes in the main molecular bands with the deprotonation. (a) carboxyl group at vacuum, (b) carboxyl group at PCM (ethanol), (c) phenolic group at vacuum, and (d) phenolic group at PCM (ethanol).

phase conditions, the CCSD results indicate a value of 1097.70 au for the first rate-dependent hyperpolarizability, β_{HRS}. Regarding the proton dissociation effect, a different behavior is observed depending on the molecular end where deprotonation occurs. Relative to the parent chromophore, the 9-pCA$^-$ molecule lost a proton from the carboxylic group and the NLO response decreased to 159.55 au, representing a divergence of 85.5%.

However, if the proton is removed from the phenolic group, the behavior is the opposite. For the 1-pCA$^-$ molecule, the value of 4191.18 au is obtained for β_{HRS}, which represents an increase of 367.3% with respect to the reference molecule (pCA). Furthermore, this effect prevails if both carboxylic and phenolic protons are removed. The CCSD predicts a higher value (1673.18 au) for the pCA^{2-} molecule than that reported for pCA.

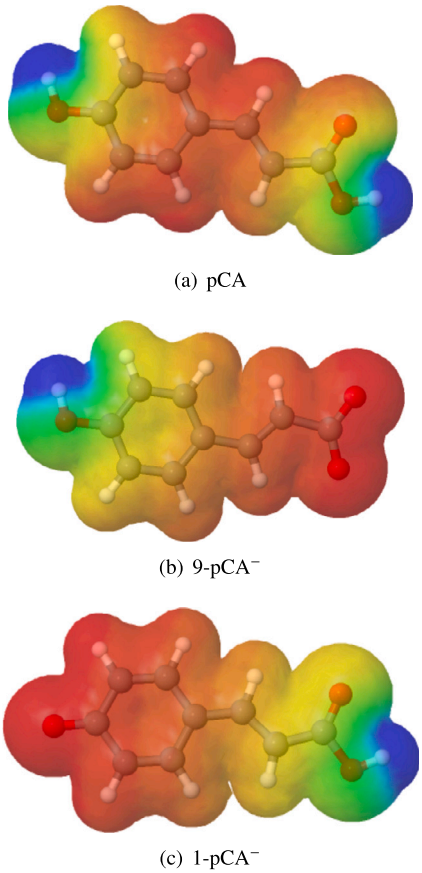

(a) pCA

(b) 9-pCA$^-$

(c) 1-pCA$^-$

Fig. 7. The molecular electrostatic potential (MEP) mapping obtained using the B3LYP/6-311++G (*d,p*) for gas-phase molecules. Blue colors denote the number of positive charges, while orange shows higher electronic density.

Based on CCSD data, the order of gain of β_{HRS} under gas phase conditions would be 9-pCA$^-$ < pCA < pCA^{2-} < 1-pCA$^-$. If we examine the other results obtained with CC2, as well as those calculated for the methods based on DFT, CAM-B3LYP, and ωB97XD, it is immediately obvious that these methods reproduce the results of CCSD at least for molecules in the gas phase. However, B3LYP gives other order of gain (9-pCA$^-$ < pCA < 1-pCA$^-$ < pCA^{2-}), which indicates that including interactions like Van der Waals and long-range corrections is essential for correct NLO description of coumarin chromophores.

Concerning the inclusion of the solvent and regardless of the dipolar or even octupolar nature of the NLO response, in general, the first hyperpolarizability presents a linear dependence with respect to the optical gap ($\beta \propto \lambda_{\mathrm{max}}$) [19,72–74]. As shown above, the experimental analysis indicates the following order for the gain of λ_{max} with respect to proton dissociation: 9-pCA$^-$ < pCA < pCA^{2-} < 1-pCA$^-$. Thus, even in a solvent environment, β_{HRS} should obey the same order, and according to the theoretical results presented in Table 4, this effect is observed. According to the CCSD/ASEC solvent approach, even in an aqueous environment, proton dissociation is key to encompassing the NLO response of pCA molecules over a wide range of values between 159.15 and 4393.97 au with all other methods, pointing to the same behavior. Regarding the performance of these materials, recent reports on the first frequency-dependent hyperpolarizability in urea and *p*-nitroaniline indicate optical responses of 37.3 and 74.3 au, respectively [76]. Therefore, pCA molecules hold promise for NLO uses.

Regarding the proper effect of the solvent, compared to CCSD and the less accurate CC2 methods and all DFT functionals present serious problems. For example, based on the relationship between β and λ_{max}, an increase in the optical response of the pCA molecule is expected, and the CCSD/ASEC and CC2/ASEC methods confirm this expectation, although predicting mild solvent effects, approximately 0.1% and 2.8%, with respect to the gas-phase value.

However, the hypochromic shift in the optical gap made for all deprotonated forms of pCA (see Table 3) indicates that the solvent should reduce the optical response. Except for the 1-pCA$^-$ molecule, CCSD and CC2 predict the correct trend for all remaining deprotonated pCA structures, but all other methods indicate an unrealistic gain in β_{HRS}. Thus, care must be taken when analyzing the NLO response of deprotonated chromophores using DFT-based methods.

It is worth making a brief comment on the effects of geometry on the NLO response of studied coumarin molecules. We calculated the NLO parameters for the gas phase and geometries in water (see **Table S5**) without accounting for the environmental contributions, and the results suggest slight geometry effects. For example, β_{HRS} values of 1373 au (11.8×10^{-30} esu) and 1414 au (12.2×10^{-30} esu) are obtained for the molecule of pCA. A similar conclusion is reached for the remaining chromophores.

Taking the CCSD approximation as a reference, DFT-based methods are known for underestimating properties like the first and second hyperpolarizabilities (β and γ). These effects have been attested for a variety of dyes like acid bases [77], cyanines [78], and *p*-quinodimethane derivatives [36]. Our results indicate that higher orders of electron-correlation effects are necessary to describe parameters like β and γ. That puts functionalities like ωB97XD, M06-2X, and B97XD at an advantageous position. For instance, looking at Table 4, B3LYP gives the poorest description of the β_{HRS} parameter. On the other hand, except for 1-pCA$^-$, the ωB97XD method is the one with the best results. Furthermore, the WB97XD functional has the advantage of providing results consistent with experimental values for different systems [80,81].

In the face of the results above, it is noteworthy to mention some probable applications. The pCA deprotonation clearly provides a switchable device with at least four operator stages. This idea is factual and has been suggested by Wang and collaborators who proposed a two-dimensional pincer with second-order nonlinear optical response modulating among at least three well-defined stages [22].

Other applications are concerned with assessing higher third-order effects from charged systems. The hyper-Rayleigh scattering allows the evaluation of the second hyperpolarizability (γ), which domains third-order effects. Moreover, the Electric Field-Induced Second Harmonic Generation (EFISHG) only can be applied to uncharged systems. However, it has been shown by theory [79] and experiment [23] that a systematic inclusion of appropriate counterions can be administrated to develop nonlinear optical switches based with higher third order coefficients (γ_{EFISHG}).

3.6. PDOS and MEP analysis

To better understand the specific effect of deprotonation on pCA molecules and to verify the influence of PCM solvent on energy levels, the Projected Density of States (PDOS) was calculated. Regarding UV-vis spectroscopy, PDOS helps to observe which molecular radicals are involved in an electronic transition [82–85]. From this work, it is clear that deprotonation has a great influence on the λ_{max}, and consequently on the β_{HRS} [19,86,87] (see section 3.4 and 3.5). Once the major molecular regions evolved into these effects, the phenolic and carboxyl groups, the PDOS was set up to observe specific changes in their bands in gas-phase and solvent PCM ethanol. This solvent has a relative permittivity value of $\epsilon = 24.5$, sufficient to observe the electrostatic interaction of the deprotonated molecules and the environment.

The PDOS of the carboxyl groups of PCA, 1-PCA$^-$ and 9-PCA$^-$ are shown in Fig. 6. Taking the pCA molecule as a reference (black line), it can be observed (Fig. 6a) that the carboxyl group has small contributions in the available states around the Highest Occupied Molecular Orbital (HOMO) ($E_{HOMO} = -6.41$ eV) and the lowest unoccupied molecular orbital (LUMO) ($E_{LUMO} = -2.12$ eV), and the relative transition is $\Delta E_{pCA} = 4.29$ eV. Relevant contributions arise at 0.0 eV and

beyond 1.50 eV. In contrast, the carboxyl of the 1-pCA$^-$ molecule (red line) has some peaks in the occupied states but is visible the importance of its orbitals in the HOMO ($E_{HOMO} = -1.51$ eV) and LUMO ($E_{LUMO} = 1.73$ eV) composition ($\Delta E_{1-pCA^-} = 3.24$ eV). Their contributions in the region of the unoccupied states are almost null, except for a faint band around 2.0 eV. In the case of the 9-pCA$^-$ molecule (blue line), the HOMO ($E_{HOMO} = -1.58$ eV) and the LUMO ($E_{LUMO} = 1.43$ eV) were shifted to higher energies, but HOMO is less sensitive than LUMO. The HOMO-LUMO gap narrowed to $\Delta E_{9-pCA} = 3.01$ eV. The emergence of the large band can be observed around −2.0 eV. Deprotonation, in these cases, shifts the energy levels to higher energies and reduces the HOMO-LUMO transition. The ethanol PCM (Fig. 6b) makes the pCA carboxyl bands broader, but there are no appreciable displacement effects. Between −6.0 eV and 0.0 eV, the 1-pCA$^-$ and 9-pCA$^-$ bands are suppressed and the redistribution of energy levels modifies the HOMO-LUMO gap: $\Delta E_{pCA} = 4.20$ eV, $\Delta E_{1-pCA^-} = 3.34$ eV, and $\Delta E_{9-pCA^-} = 4.62$ eV. This difference in the band gap for 9-pCA$^-$ from gas-phase to ethanol confirms the sensitivity of the deprotonated radical to electrostatic effects.

The analysis of the phenolic group in a gas phase is shown in Fig. 6c. As can be seen, the associated bands have the majority of states available for occupation. In the case of the pCA molecule, the phenolic group (black line) has a small contribution to the HOMO composition, but peaks around −2.0 eV are contributing to LUMO. The bands in the region of the unoccupied orbitals are shifted to lower energies. Compared to the gas-phase results, there is a higher PDOS throughout the analyzed energy range and the bands are more dense. The same conclusion could be reached for 1-pCA$^-$ (red lines) and 9-pCA$^-$ (blue line). Since these results are on different regions of the same molecules, and if these curves are put together, it can be seen that the phenolic group is more prominent and their contributions are complementary. It occurs due to the larger number of π electrons in the phenolic group and the presence of oxygen, which is an electron attractor. For 1-pCA$^-$ the trend of the band extends throughout the energy interval and for 9-pCA$^-$ the central bands are suppressed and redistributed in order to concentrate their peaks and increase the degeneracy in their bands. When the effect of PCM solvent is taken into account (Fig. 6d) the separation between the contributions of HOMO-LUMO to PDOS for 1-pCA$^-$ and 9-pCA$^-$ becomes clear. The pCA molecule is less sensitive to the PCM solvent. It shows the sensitivity of the phenolic group to electrostatic effects and the shift of the bands at lower energies. A large band is shown by 1-pCA$^-$ and 9-pcA$^-$ in the region of unoccupied orbitals.

In summary, the redistribution of molecular energy levels under deprotonation shows that the phenolic group is determinant in the dynamics of electronic transitions. Despite the contributions of π-electrons from the carboxyl group and from the central chain of atoms, the phenolic group shows sensitivity to deprotonation even in the 9-pCA$^-$ molecule. Once these dynamics change the electronic transitions, it is associated with the change of the NLO response of these molecules through the loss of H atoms in the phenolic and carboxyl groups.

Molecular electrostatic potential (MEP) plots, Fig. 7, for the neutral pCA molecule, and its two monoanionic forms, is another way to understand the effect of proton removal. As can be seen, the removal of the H atom from the phenyl group attracts the electron density onto the phenyl ring, in agreement with the prediction aforementioned in the PDOS analysis.

3.7. Dipolar and octupolar contributions

The NLO response of a chromophore is composed of dipolar ($\Phi_{J=1}$) and octupolar ($\Phi_{J=3}$) contributions [19], and it is important to know which is predominant to propose suitable NLO applications. Therefore, to better classify the optical response of pCA molecules, **Table S6** presents the CAM-B3LYP results for these contributions obtained in both gas and solvent.

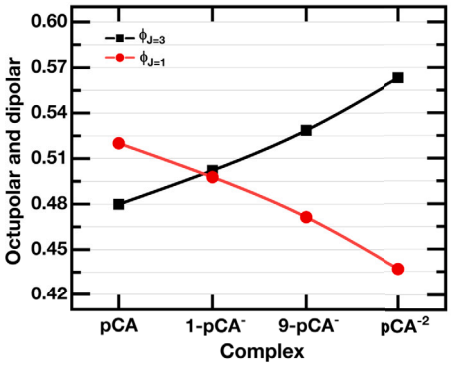

(a) Gas-phase molecules

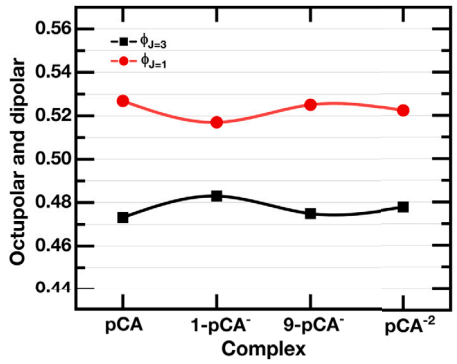

(b) Hydrated molecules (ASEC)

Fig. 8. The octupolar ($\Phi_{J=3}$) and dipolar ($\Phi_{J=1}$) contributions plotted for the pCA molecules at gas-phase (top) and in an aqueous solvent (bottom).

Under gas phase conditions, Fig. 8a allows us to see the effect of proton dissociation. The neutral pCA molecule is essentially a dipole ($\Phi_{J=1} > \Phi_{J=3}$). However, systematic removal of the proton from any hydroxide group reverses this condition, making the system slightly more octupolar ($\Phi_{J=1} < \Phi_{J=3}$). The same behavior is attested by the concept of depolarization ratio (DR), in which the values range from 1.5 (dipolar) to 9 (octupolar) values. According to **Table S3**, from pCA to pCA^{2-}, the DR values decrease from 4.55 to 3.45, indicating a predominance of dipolar architectures with deprotonation.

This effect occurs by reducing the dimensions of the molecules in a preferential direction by removing the hydrogen from the hydroxyl groups. This process makes the chromophores more three-dimensional, which favors the charge transfer procedure in all molecular axes, becoming octupolar [50,75].

However, the effect of the solvent is opposite to that observed above. Fig. 8b clearly shows that dipolar contributions prevail in the liquid environment for all pCA derivatives. This effect probably has its origin in the polarization of the solute due to the solvent, which for ground-state molecules, can increase the permanent molecular dipole moment. For nearly one-dimensional molecules such as the pCA derivatives shown in Fig. 1, this behavior favors unidirectional charge transfer procedures on a preferential molecular axis, which is conduction for the establishment of dipole contributions.

4. Conclusions

We have carried out a systematic investigation of the effects of solvent and deprotonation on the thermochemical stability, solvatochromism, and NLO response of the pCA molecule and its deprotonated derivatives. The solvent has a large impact on the optical response. The UV-Vis spectra of all deprotonated forms of pCA undergo a blue shift from gas to solvent, while the neutral pCA molecule un-

dergoes a bathochromic shift. As a general behavior, dissociation of the proton changes the absorption maximum within a wide range of values ($285 \leq \lambda_{max} \leq 356$ nm) in the visible spectrum. However, the impact on the NLO response is more pronounced. The used QM methods indicate that these properties are primarily sensitive to the molecular periphery from which the proton is extracted *i.e.* the outer molecular electronic cloud. An ionization in the carboxylic group leads to higher optical gaps and the lowest NLO response. On the other hand, if the extraction occurs in the phenolic group, lower values of the absorption maximum and giant values of the NLO coefficients are observed. Solvated CCSD calculations show a large value ($159.15 \leq \beta_{HRS} \leq 4393.9$ au) which is significant for the modulation of the second-order NLO response. From the QM point of view, this effect occurs because the preferential removal of protons affects the contribution of the π conducting orbitals located in the aromatic ring. As a general conclusion, proton dissociation works as an NLO switch considerably improving the NLO behavior of pCA molecules. Thermochemical analysis indicated that the two non-ionic structures (9-pCA$^-$ and 1-pCA$^-$) are stable in a solvent, allowing a wide range of NLO modulations.

CRediT authorship contribution statement

All the authors contributed equally.

Declaration of competing interest

The authors declare that they have no known competing financial interests or personal relationships that could have appeared to influence the work reported in this paper.

Data availability

No data was used for the research described in the article.

Acknowledgements

This study was financed in part by the Coordenação de Aperfeiçoamento de Pessoal de Nível Superior - Brasil (CAPES) - Finance Code 001, Conselho Nacional de Desenvolvimento Científico e Tecnológico (CNPq) 102225/2022-2. PFP and GIP would like to acknowledge financial support from CONICET, PIP 11220200100467CO. GIP received funds from Universidad de Buenos Aires, UBACYT 20020170100456BA and PFP from FaCENA-UNNE, PI 21F015 Res. N° 776-21 CS.

Appendix A. Supplementary material

Supplementary material related to this article can be found online at https://doi.org/10.1016/j.molliq.2023.123587.

References

[1] M. Marinescu, Synthesis and nonlinear optical studies on organic compounds in laser-deposited films, in: Applied Surface Science, IntechOpen, 2019, https://doi.org/10.5772/intechopen.83234.
[2] C. Reichardt, Solvent Effects in Organic Chemistry, Verlag Chemie, Weinheim, New York, 1979.
[3] C. Reichardt, Solvatochromic dyes as solvent polarity indicators, Chem. Rev. 94 (1994) 2319–2358, https://doi.org/10.1021/cr00032a005.
[4] C. Reichardt, Empirical parameters of the polarity of solvents, Angew. Chem. 4 (1965) 29–40, https://doi.org/10.1002/anie.196500291.
[5] G.C. Maitland, M. Rigby, E.B. Smith, W.A. Wakeham, Intermolecular Forces-Their Origin and Determination, Oxford University Press, Oxford, 1987.
[6] H. Ratajczak, W.J. Orville-Thomas, Molecular Interactions, vol. 1–3, Wiley, New York, 1980–1982.
[7] S.N. Timasheff, Protein-solvent interactions and protein conformation, Acc. Chem. Res. 3 (1970) 62–68, https://doi.org/10.1021/ar50026a004.
[8] P. Suppan, N. Ghoneim, Solvatochromism, The Royal Society of Chemistry, London, 1997.
[9] S.E. Sheppard, The effects of environment and aggregation on the absorption spectra of dyes, Rev. Mod. Phys. 14 (1942) 303, https://doi.org/10.1103/RevModPhys.14.303.
[10] W.L. Archer, Industrial Solvents Handbook, Dekker, New York, 1996.
[11] R. Alfano, Y. Pu, 11 - Optical biopsy for cancer detection, Lasers Med. Appl. (2013) 325–367, https://doi.org/10.1533/9780857097545.3.325.
[12] A. Katz, R.R. Alfano, Stokes shift spectroscopy for biomedical applications and bioagent sensing, in: Digest of the LEOS Summer Topical Meetings Biophotonics/Optical Interconnects and VLSI Photonics/WBM Microcavities, IEEE, 2004.
[13] T.H. Maiman, Stimulated optical radiation in ruby, Nature 187 (1960) 493–494, https://doi.org/10.1038/187493a0.
[14] T. Schneider, Nonlinear Optics in Telecommunications, Springer Berlin Heidelberg, 2004.
[15] J. Moloney, Nonlinear Optics, CRC Press, Taylor & Francis Group, Boca Raton, FL, 2018.
[16] H. Xu, D.L. Elder, L.E. Johnson, B.H. Robinson, L.R. Dalton, Molecular engineering of structurally diverse dendrimers with large electro-optic activities, ACS Appl. Mater. Interfaces 11 (23) (2019) 21058–21068, https://doi.org/10.1021/acsami.9b05306.
[17] J. Huang, Y. Yang, J. He, Z. He, H. Wu, The important role of tetraphenylethene on designing bichromophores for organic nonlinear optical materials, Mater. Lett. 291 (2021) 129521, https://doi.org/10.1016/j.matlet.2021.129521.
[18] S.R. Marder, Organic nonlinear optical materials: where we have been and where we are going, Chem. Commun. (2006) 131–134, https://doi.org/10.1039/B512646K.
[19] D.R. Kanis, M.A. Ratner, J.T. Marks, Design and construction of molecular assemblies with large second-order optical nonlinearities. Quantum chemical aspects, Chem. Rev. 94 (1994) 195, https://doi.org/10.1021/cr00025a007.
[20] R. Bano, M. Asghar, K. Ayub, T. Mahmood, J. Iqbal, S. Tabassum, R. Zakaria, M.A. Gilani, A theoretical perspective on strategies for modeling high performance nonlinear optical materials, Front. Mater. 8 (2021), https://doi.org/10.3389/fmats.2021.783239.
[21] M. Papadopoulos, Non-linear Optical Properties of Matter: From Molecules to Condensed Phases, Springer, Dordrecht, 2006.
[22] C.H. Wang, N.N. Ma, X.X. Sun, S.L. Sun, Y.Q. Qiu, P.J. Liu, Modulation of the second-order nonlinear optical properties of the two-dimensional pincer Ru(II) complexes: substituent effect and proton abstraction switch, J. Phys. Chem. A 116 (2012) 10496–10506, https://doi.org/10.1021/jp3062288.
[23] F. Nisic, A. Colombo, Claudia Dragonetti, M. Fontani, D. Marinotto, S. Righetto, D. Roberto, J.A. Gareth Williams, Highly efficient acido-triggered reversible luminescent and nonlinear optical switch based on 5-π-delocalized-donor-1, 3-di(2-pyridyl)benzenes, J. Mater. Chem. C 3 (2015) 7421–7427, https://doi.org/10.1039/C5TC01529D.
[24] A.C.M. Pimenta, T. Andrade-Filho, V. Manzoni, J. Del Nero, R. Gester, Giant values obtained for first hyperpolarizabilities of methyl orange: a DFT investigation, Theor. Chem. Acc. 138 (2019) 27, https://doi.org/10.1007/s00214-018-2406-x.
[25] V. Manzoni, L. Modesto-Costa, J. Del Nero, T. Andrade-Filho, R. Gester, Strong enhancement of NLO response of methyl orange dyes through solvent effects: a sequential Monte Carlo/DFT investigation, Opt. Mater. 94 (2019) 152–159, https://doi.org/10.1016/j.optmat.2019.05.018.
[26] K. Pei, J. Ou, J. Huang, S. Ou, p-Coumaric acid and its conjugates: dietary sources, pharmacokinetic properties and biological activities, J. Sci. Food Agric. 96 (2016) 2952–2962, https://doi.org/10.1002/jsfa.7578.
[27] R.G. Parr, W. Yang, Density Functional Theory of Atoms and Molecules, Oxford Science Publications, 1994.
[28] P. Hohenberg, W. Kohn, Inhomogeneous electron gas, Phys. Rev. 136 (1964) B864–B871, https://doi.org/10.1103/PhysRev.136.B864.
[29] W. Kohn, L.J. Sham, Self-consistent equations including exchange and correlation effects, Phys. Rev. 140 (1965) A1133–A1138, https://doi.org/10.1103/PhysRev.140.A1133.
[30] A.D. Becke, Density-functional thermochemistry. III. The role of exact exchange, J. Chem. Phys. 98 (1993) 5648–5652, https://doi.org/10.1063/1.464913.
[31] C. Lee, W. Yang, R.G. Parr, Development of the Colle-Salvetti correlation-energy formula into a functional of the electron density, Phys. Rev. B 37 (1988) 785–789, https://doi.org/10.1103/physrevb.37.785.
[32] Chr Møller, M.S. Plesset, Note on an approximation treatment for many-electron systems, Phys. Rev. 46 (1934) 618, https://doi.org/10.1103/PhysRev.46.618.
[33] T. Clark, J. Chandrasekhar, G.W. Spitznagel, P.R. Schleyer, Efficient diffuse function-augmented basis sets for anion calculations. III. The 3-21+G basis set for first-row elements, Li-F, J. Comput. Chem. 4 (1983) 294–301, https://doi.org/10.1002/jcc.540040303.
[34] R. Krishnan, J.S. Binkley, R. Seeger, J.A. Pople, Self-consistent molecular orbital methods. XX. A basis set for correlated wave functions, J. Chem. Phys. 72 (1980) 650–654, https://doi.org/10.1063/1.438955.
[35] M. de Wergifosse, B. Champagne, Electron correlation effects on the first hyperpolarizability of push-pull π-conjugated systems, J. Chem. Phys. 134 (2011) 134074113, https://doi.org/10.1063/1.3549814.
[36] M. Wergifosse, F. Wautelet, B. Champagne, R. Kishi, K. Fukuda, H. Matsui, M. Nakano, Challenging compounds for calculating hyperpolarizabilities: p-quinodimethane derivatives, J. Phys. Chem. A 117 (2013) 4709, https://doi.org/10.1021/jp403163z.

[37] C. Fiolhais, F. Nogueira, M. Marques (Eds.), A Primer in Density Functional Theory, Springer, 2003, Chapter 4.
[38] M.J. Frisch, et al., Gaussian 09, Revision A.02, Gaussian Inc., Wallingford CT, 2016.
[39] S. Miertus, E. Scrocco, J. Tomasi, Electrostatic interaction of a solute with a continuum. A direct utilization of AB initio molecular potentials for the prevision of solvent effects, Chem. Phys. 55 (1981) 117–129, https://doi.org/10.1016/0301-0104(81)85090-2.
[40] S. Miertu, J. Tomasi, Approximate evaluations of the electrostatic free energy and internal energy changes in solution processes, Chem. Phys. 65 (1982) 239, https://doi.org/10.1016/0301-0104(82)85072-6.
[41] R.C. Guedes, K. Coutinho, B.J. Costa Cabral, S. Canuto, C.F. Correia, R.M.B. dos Santos, J.A.M. Simões, Solvent effects on the energetics of the phenol O-H bond: differential solvation of phenol and phenoxy radical in benzene and acetonitrile, J. Phys. Chem. A 107 (2003) 9197–9207, https://doi.org/10.1021/jp035912c.
[42] H.C. Georg, S. Canuto, Electronic properties of water in liquid environment. A sequential QM/MM study using the free energy gradient method, J. Phys. Chem. B 116 (2012) 11247–11254, https://doi.org/10.1021/jp304201b.
[43] R.M. Gester, H.C. Georg, S. Canuto, M.C. Caputo, P.F. Provasi, NMR chemical shielding and spin-spin coupling constants of liquid NH3: a systematic investigation using the sequential QM/MM method, J. Phys. Chem. A 113 (2009) 14936–14942, https://doi.org/10.1021/jp9050484.
[44] N. Metropolis, A.W. Rosenbluth, M.N. Rosenbluth, A.H. Teller, E. Teller, Equation of state calculations by fast computing machines, J. Chem. Phys. 21 (1953) 1087, https://doi.org/10.1063/1.1699114.
[45] W.R. Rocha, K.J. de Almeida, K. Coutinho, S. Canuto, An efficient quantum mechanical/molecular mechanics Monte Carlo simulation of liquid water, Chem. Phys. Lett. 335 (2001) 127–133, https://doi.org/10.1016/S0009-2614(01)00024-0.
[46] M.P. Allen, D.J. Tildesley, Computer Simulation of Liquids, Clarendon, Oxford, 1987.
[47] H.J.C. Berendsen, J.P.M. Postma, W.F. van Gunsteren, J. Hermans, in: B. Pullman (Ed.), Intermolecular Forces, Reidel, Dordrecht, 1981.
[48] W.L. Jorgensen, D.S. Maxwell, J. Tirado-Rives, Development and testing of the OPLS all-atom force field on conformational energetics and properties of organic liquids, view author information, J. Am. Chem. Soc. 118 (1996) 11225–11236, https://doi.org/10.1021/ja9621760.
[49] K. Coutinho, H. Georg, T. Fonseca, V. Ludwig, S. Canuto, An efficient statistically converged average configuration for solvent effects, Chem. Phys. Lett. 437 (2007) 148, https://doi.org/10.1016/j.cplett.2007.02.012.
[50] L. Zhang, D. Qi, L. Zhao, C. Chen, Y. Bian, W. Li, Density functional theory study on subtriazaporphyrin derivatives: dipolar/octupolar contribution to the second-order nonlinear optical activity, J. Phys. Chem. A 116 (2012) 10249, https://doi.org/10.1021/jp3079293.
[51] B. Champagne, P. Beaujean, M. de Wergifosse, M. Hidalgo Cardenuto, V. Liégeois, F. Castet, Quantum chemical methods for predicting and interpreting second-order nonlinear optical properties: from small to extended π-conjugated molecules, in: Frontiers of Quantum Chemistry, Springer, Singapore, 2017, pp. 117–138.
[52] A. Plaquet, M. Guillaume, B. Champagne, F. Castet, L. Ducasse, J.L. Pozzo, V. Rodriguez, In silico optimization of merocyanine-spiropyran compounds as second-order nonlinear optical molecular switches, Phys. Chem. Chem. Phys. 10 (2008) 6223–6232, https://doi.org/10.1039/B806561F.
[53] K. Aidas, et al., The Dalton quantum chemistry program system, Wiley Interdiscip. Rev. Comput. Mol. Sci. 4 (2013) 269–284, https://doi.org/10.1002/wcms.1172.
[54] T. Lu, F. Chen, Multiwfn: a multifunctional wavefunction analyzer, J. Comput. Chem. 33 (2012) 580, https://doi.org/10.1002/jcc.22885.
[55] D. Zuev, K.B. Bravaya, T.D. Crawford, R. Lindh, A.I. Krylov, Electronic structure of the two isomers of the anionic form of p-coumaric acid chromophore, J. Chem. Phys. 134 (2011) 034310, https://doi.org/10.1063/1.3516211.
[56] F.F. García-Prieto, I.F. Galvá, A. Muñoz-Losa, M.A. Aguilar, M.E. Martín, Solvent effects on the absorption spectra of the para-coumaric acid chromophore in its different protonation forms, J. Chem. Theory Comput. 9 (2013) 4481, https://doi.org/10.1021/ct400145z.
[57] R. Świsłocka, M. Kowczyk-Sadowy, M. Kałinowska, W. Lewandowski, Spectroscopic (FT-IR, FT-Raman, ^{1}H and ^{13}C NMR) and theoretical studies of p-coumaric acid and alkali metal p-coumarates, Spectroscopy 27 (2012) 35, https://doi.org/10.3233/SPE-2012-0568.
[58] R.F. Bryan, P.G. Forcier, Contrasting solid-state structures for two nematogenic benzylideneanilines. Crystal structures of p [(p'-ethoxybenzylidene)amino] -benzonitrile and p- [(p'-methoxybenzylidene)amino] -phenyl acetate, Mol. Cryst. Liq. Cryst. 60 (1980) 157, https://doi.org/10.1080/00268948008072429.
[59] N. Schultheiss, M. Roea, S.X.M. Boerrigtera, Cocrystals of nutraceuticalp-coumaric acid with caffeine and theophylline: polymorphism and solid-state stability explored in detail using their crystal graphs, CrystEngComm 13 (2011) 611, https://doi.org/10.1039/C0CE00214C.
[60] H. Rodríguez, I. Angulo, B. de las Rivas, N. Campillo, J.A. Páez, R. Muñoz, J.M. Mancheño, p-Coumaric acid decarboxylase from lactobacillus plantarum: structural insights into the active site and decarboxylation catalytic mechanism 78 (2010) 1662, https://doi.org/10.1002/prot.22684.
[61] M. Boggio-Pasqua, G. Groenhof, Controlling the photoreactivity of the photoactive yellow protein chromophore by substituting at the p-coumaric acid group, J. Phys. Chem. B 115 (2011) 7021, https://doi.org/10.1021/jp108977x.
[62] A.R. da Cunha, E.L. Duarte, M.T. Lamy, K. Coutinho, Protonation/deprotonation process of Emodin in aqueous solution and pK a determination: UV/visible spectrophotometric titration and quantum/molecular mechanics calculations, Chem. Phys. 440 (2014) 69, https://doi.org/10.1016/j.chemphys.2014.06.009.
[63] G.J. Tawa, I.A. Topol, S.K. Burt, Calculation of the aqueous solvation free energy of the proton, J. Chem. Phys. 109 (1998) 4852, https://doi.org/10.1063/1.477096.
[64] P.K. Kelly, C.J. Cramer, D.G. Truhlar, Aqueous solvation free energies of ions and ion-water clusters based on an accurate value for the absolute aqueous solvation free energy of the proton, J. Phys. Chem. B 110 (2006) 16066, https://doi.org/10.1021/jp063552y.
[65] D.M. Camaioni, C.A. Schwerdtfeger, Comment on "Accurate experimental values for the free energies of hydration of H+, OH-, and H3O+", J. Phys. Chem. A 109 (2005) 10795, https://doi.org/10.1021/jp054088k.
[66] C.G. Zhan, D.A. Dixon, First-principles determination of the absolute hydration free energy of the hydroxide ion, J. Phys. Chem. A 106 (2002) 9737, https://doi.org/10.1021/jp014533l.
[67] C.G. Zhan, D.A. Dixon, Absolute hydration free energy of the proton from first-principles electronic structure calculations, J. Phys. Chem. A 105 (2001) 11534, https://doi.org/10.1021/jp012536s.
[68] M.D. Tissandier, K.A. Cowen, W.Y. Feng, E. Gundlach, M.J. Cohen, A.D. Earhart, J.V. Coe, The proton's absolute aqueous enthalpy and Gibbs free energy of solvation from cluster-ion solvation data, J. Phys. Chem. A 102 (1998) 7787, https://doi.org/10.1021/jp982638r.
[69] Y. Marcus, Ion Solvation, Wiley, New York, 1985.
[70] J.L. Beltrán, N. Sanli, G. Fonrodona, D. Barrón, G. Özkan, J. Barbosa, Spectrophotometric, potentiometric and chromatographic pKa values of polyphenolic acids in water and acetonitrile–water media, Anal. Chim. Acta 484 (2003) 253, https://doi.org/10.1016/S0003-2670(03)00334-9.
[71] P. Changenet-Barret, A. Espagne, S. Charier, J.B. Baudin, L. Jullien, P. Plaza, K.J. Hellingwerf, M.M. Martin, Early molecular events in the photoactive yellow protein: role of the chromophore photophysics, Photochem. Photobiol. Sci. 3 (2004) 823, https://doi.org/10.1039/B400398E.
[72] L.T. Cheng, W. Tam, S.H. Stevenson, G.R. Meredith, G. Rikken, S.R. Marder, Experimental investigations of organic molecular nonlinear optical polarizabilities. 1. Methods and results on benzene and stilbene derivatives, J. Phys. Chem. 95 (1991) 10631, https://doi.org/10.1021/j100179a026.
[73] D.M. Burland, J.E. Rice, M. Stähelin, Molecular systems for nonlinear optical applications, molecular crystals and liquid crystals, Sci. Technol. 216 (2006) 27, https://doi.org/10.1080/10587259208028744.
[74] R. Gester, A. Torres, C. Bistafa, R.S. Araújo, T.A. da Silva, V. Manzoni, Theoretical study of a recently synthesized azo dyes useful for OLEDs, Mater. Lett. 280 (2020) 128535, https://doi.org/10.1016/j.matlet.2020.128535.
[75] S. Fonseca, N.S.S. dos Santos, A.R. da Cunha, S. Canuto, P.F. Provasi, T. Andrade-Filho, R. Gester, The solute polarization and structural effects on the nonlinear optical response of based chromone molecules, ChemPhysChem (2023), https://doi.org/10.1002/cphc.202300060.
[76] R. Gester, M. Siqueira, A.R. Cunha, R.S. Araújo, P.F. Provasi, S. Canuto, Assessing the dipolar-octupolar NLO behavior of substituted thiosemicarbazone assemblies, Chem. Phys. Lett. 831 (2023) 140807, https://doi.org/10.1016/j.cplett.2023.140807.
[77] A. Alparone, Linear and nonlinear optical properties of nucleic acid bases, Chem. Phys. 410 (2013) 90, https://doi.org/10.1016/j.chemphys.2012.11.005.
[78] L. Xu, A. Kumar, B.M. Wong, Linear polarizabilities and second hyperpolarizabilities of streptocyanines: results from broken-symmetry DFT and New CCSD(T) benchmarks, J. Comput. Chem. 39 (2018) 2350, https://doi.org/10.1002/jcc.25519.
[79] T.N. Ramos, S. Canuto, B. Champagne, Unraveling the electric field-induced second harmonic generation responses of stilbazolium ion pairs complexes in solution using a multiscale simulation method, J. Chem. Inf. Model. 60 (2020) 4817, https://doi.org/10.1021/acs.jcim.9b01161.
[80] Renato Barbosa-Silva, Manoel L. Silva-Neto, Dipankar Bain, Lucas Modesto-Costa, Tarciso Andrade-Filho, Vinícius Manzoni, Amitava Patra, Cid B. de Araújo, J. Phys. Chem. C 124 (2020) 15440–15447, https://doi.org/10.1021/acs.jpcc.0c03397.
[81] R. Barbosa-Silva, M.S.S. Oliveira, R.C. Ferreira, V. Manzoni, E.H.L. Falcão, C.B. de Araújo, Opt. Mater. 146C (2023) 114536, https://doi.org/10.1016/j.optmat.2023.114536.
[82] L. Zhang, K. Xu, Understanding substitution effects on dye structures and optoelectronic properties of molecular halide perovskite Cs4MX6 (M = Pb, Sn, Ge; X= Br, I, Cl), J. Mol. Graph. Model. 91 (2019) 172–179, https://doi.org/10.1016/j.jmgm.2019.06.009.
[83] D.F.S. Ferreira, W.D. Oliveira, E. Belo, R. Gester, M.R.S. Siqueira, A.M.J.C. Neto, J. Del Nero, Electron scattering processes in steroid molecules via NEGF-DFT: the opening of conduction channels by central oxygen, J. Mol. Graph. Model. 101 (2020) 107755, https://doi.org/10.1016/j.jmgm.2020.107755.
[84] B. Badhani, R. Kakkar, et al., A DFT-D2 study on the adsorption of phosgene derivatives and chloromethyl chloroformate on pristine and Fe4-decorated graphene, J. Mol. Graph. Model. 101 (2020) 107754, https://doi.org/10.1016/j.jmgm.2020.107754.
[85] A.M. Rodrigues, A.R. Palheta-Júnior, M.S.S. Pinheiro, A.M.R. Marinho, A.M.J. Chaves-Neto, R. Gester, T. Andrade-Filho, Encapsulation ability of silicon carbide and boron nitride nanotubes for spilanthol molecule, J. Nanostruct. Chem. 11 (2021) 203–213, https://doi.org/10.1007/s40097-020-00359-5.

[86] L.T. Cheng, W. Tam, S.H. Stevenson, G.R. Meredith, G. Rikken, S.R. Marder, Experimental investigations of organic molecular nonlinear optical polarizabilities. 1. Methods and results on benzene and stilbene derivatives, J. Phys. Chem. 95 (1991) 10631–10643, https://doi.org/10.1021/j100179a026.

[87] D.M. Burland, J.E. Rice, M. Stähelin, Molecular systems for nonlinear optical applications, Mol. Cryst. Liq. Cryst. Sci. Technol., Sect. A Mol. Cryst. Liq. Cryst. 216 (1992) 27–32, https://doi.org/10.1080/10587259208028744.

[88] H.C. Georg, K. Coutinho, S. Canuto, Solvent effects on the UV-visible absorption spectrum of benzophenone in water: a combined Monte Carlo quantum mechanics study including solute polarization, J. Chem. Phys. 126 (2007) 034507, https://doi.org/10.1063/1.2426346.

[89] H.M. Cezar, S. Canuto, K. Coutinho, DICE: a Monte Carlo code for molecular simulation including the configurational bias Monte Carlo method, J. Chem. Inf. Model. 60 (2020) 3472–3488, https://doi.org/10.1021/acs.jcim.0c00077.

[90] P. Zhou, F. Tian, F. Lv, Z. Shang, Geometric characteristics of hydrogen bonds involving sulfur atoms in proteins, Proteins, Struct. Funct. Bioinform. 76 (2008) 151, https://doi.org/10.1002/prot.22327.

[91] R. Kumar, J.R. Schmidt, J.L. Skinner, Hydrogen bonding definitions and dynamics in liquid water, J. Chem. Phys. 126 (2007) 204107, https://doi.org/10.1063/1.2742385.

[92] V.R.R. Cunha, V.R.L. Constantino, R.A. Ando, Raman spectroscopy and DFT calculations of para-coumaric acid and its deprotonated species, Vib. Spectrosc. 58 (2012) 139, https://doi.org/10.1016/j.vibspec.2011.12.007.

[93] T. Rocha-Rinza, et al., Gas phase absorption studies of photoactive yellow protein chromophore derivatives, J. Phys. Chem. A 113 (2009) 9442, https://doi.org/10.1021/jp904660w.